J. Fluid Mech. (2012), *vol.* 701, *pp.* 460–472. © Cambridge University Press 2012
doi:10.1017/jfm.2012.181

Mass transport under standing waves over a sloping beach

Pietro Scandura[1]†, Enrico Foti[1] and Carla Faraci[2]

[1] Department of Civil and Environmental Engineering, University of Catania, Viale A. Doria 6, 95125 Catania, Italy

[2] Department of Civil and Environmental Engineering, University of Messina, C.da Di Dio (S. Agata), 98166 Messina, Italy

(Received 29 October 2011; revised 22 March 2012; accepted 11 April 2012; first published online 14 May 2012)

This paper deals with the mass transport induced by sea waves propagating over a sloping beach and fully reflected from a wall. It is shown that for moderate slopes the classical recirculation cell structure holds for small Reynolds numbers only. When the Reynolds number is large, the cells interact among themselves giving rise to the merging of the negative cells and the confinement of the positive ones near the bottom. Under such circumstances the fluid moves onshore near the bottom and offshore near the free surface. The seaward decrease of the vorticity produced at the bottom appears to be the reason for the merging phenomenon.

Key words: boundary layers, coastal engineering, surface gravity waves

1. Introduction

Water particles under surface gravity waves possess, apart from their predominant oscillating motion, a second-order mean velocity called mass transport. Although such a mean flow is weak compared with the oscillating component, it plays an important role in transport processes.

In the core region of the water column the mass transport is strongly influenced by the steady streaming in the boundary layers, as demonstrated theoretically by Longuet-Higgins (1953). He showed that, when the fluid viscosity is taken into account, a second-order mean Eulerian velocity is generated near the bed, which persists at the outer edge of the boundary layer. The theory shows that in the free surface boundary layer a mean vorticity is generated as well, which persists beyond this layer (Longuet-Higgins 1953; Liu 1977). A discussion about the generation of steady streaming in several different contexts is reported in the review paper of Riley (2001).

In the core region the mass transport is described by a convection–diffusion equation (Longuet-Higgins 1953; Dore 1976) in which the order of magnitude of the ratio between the diffusive and the convective terms is given by $D = (\delta/a_0)^2/2$, where a_0 is the wave amplitude and δ the boundary layer thickness. The parameter D can be regarded as the inverse of a Reynolds number.

In the case of progressive waves propagating over a constant depth, the convective term can be neglected, then the mass transport velocity in the core can be computed

† Email address for correspondence: pscandu@dica.unict.it

https://doi.org/10.1017/jfm.2012.181 Published online by Cambridge University Press

by the analytical diffusion solution of Longuet-Higgins (1953). Craik (1982) showed that the wave attenuation can significantly modify the diffusion solution only when the attenuation length scale is comparable with the water depth. However, in the case of an uneven bottom, the convective term must be considered unless we are in the very unusual situation where the wave amplitude a_0 is much smaller than the thickness of the Stokes boundary layer δ. In the field and in many laboratory experiments, inertia prevails over viscous forces everywhere in the fluid domain except in a region, denoted as the second boundary layer, where they are of the same order of magnitude (Dore 1976).

Under standing waves the mass transport is characterized by recirculating cells. In the case of an horizontal bottom, the structure of this flow has been studied by Longuet-Higgins (1953) for $D \gg 1$ and numerically by Haddon & Riley (1983) for the case $D = O(1)$. Numerical results for waves which are partially reflected are reported by Iskandarani & Liu (1991*a*,*b*) and Wen & Liu (1994).

The case of waves propagating over a sloping bottom, although of great interest, has been investigated in few studies. Hunt & Johns (1963) developed formulas to compute the steady streaming in the bottom boundary layer of three-dimensional waves over a generic bottom, although they did not consider the flow in the core region. Carter, Liu & Mei (1973) used the previous formulas to compute the mass transport under a sea wave partially reflected from the beach. Lau & Travis (1973) computed the mass transport in the bottom boundary layer of a sea wave propagating over a gently sloping beach and partially reflected, in order to clarify the formation mechanism of sand bars parallel to the coast. In such study the wavefield was computed by the geometrical optics approximation, which is strictly valid when the slope is much smaller than the ratio between the water depth h and the wavelength λ (Mei, Stiassnie & Yue 2005*a*).

More recently, Blondeaux, Brocchini & Vittori (2002) developed a mathematical model, based on the shallow water approximation and on the assumption of waves of small steepness, to compute the mass transport under sea waves propagating over a sloping beach. Then, both the ratio h/λ and the bottom slope were assumed much smaller than 1.

The aim of the present work is to study the mass transport due to waves propagating over a sloping beach and fully reflected from a wall. An appropriate mathematical model was specifically developed in which the main restriction is due to the assumption of a wave steepness much smaller than 1. The flow is assumed laminar and the thickness of the Stokes layer much smaller than the characteristic dimension of the fluid domain. The advancement with respect to the model of Blondeaux *et al.* (2002) is due to two reasons. The first is the use of the exact irrotational linear wave theory to determine the flow at the leading order of approximation in the core region. Indeed, this choice avoids restrictions on the values of the beach slope, such those arising by using the shallow water or the geometrical optics approximations. The second is the maintenance of the viscous diffusion in the cross-shore direction in the governing equations, which plays an important role when describing the vorticity dynamics under standing waves.

2. Formulation of the problem and solution procedure

Let us consider a plane sloping beach and a two-dimensional sinusoidal wave of angular frequency σ^* propagating in the direction normal to the coast. Hereinafter an asterisk denotes a dimensional variable. The reference system has the origin in the shoreline, the x^*-axis lying on the still water level, orthogonal to the coastline and

https://doi.org/10.1017/jfm.2012.181 Published online by Cambridge University Press

pointing offshore and the y^*-axis vertical and pointing upwards. In deep water the incoming wave has an amplitude a_0^* and a wavenumber k_0^*. In this study the lengths are scaled by $1/k_0^*$, the vertical displacement of the free surface η^* by a_0^*, the velocities (u^*, v^*) by $\sigma^* a_0^*$ and the time t^* by $1/\sigma^*$. Most of the analysis reported in this section is rather known in literature, therefore we outline only the main results.

Present flow is characterized by three dimensionless parameters: a_0, δ and the bottom slope β. The parameter $a_0 = a_0^* k_0^*$ provides a measure of the importance of the wave nonlinearity. We assume that a_0 is much smaller than 1 as this is an appropriate hypothesis outside the surf zone. The parameter $\delta = k_0^* \sqrt{2\nu^*/\sigma^*}$, where ν^* is the kinematic viscosity, is proportional to the ratio between the thickness of the Stokes layer and the wavelength, thus representing a measure of the importance of the viscous effects. Usually this parameter is much smaller than one, then to a first approximation the viscous effects are negligible, except in the boundary layers.

The solution procedure begins by expanding the variables in a double power series of the small parameters a_0 and δ. By substituting such expansion in the Navier–Stokes equations and in the boundary conditions, as expected, it emerges that at the leading order of approximation the flow in the core region is irrotational. Since we consider only solutions that are periodic in time, the potential function Φ can be written as $\Phi = \mathrm{Re}(\mathrm{e}^{\mathrm{i}t}\varphi(x, y))$, where i is the imaginary unit and Re means real part. The potential φ satisfies the Laplace equation and the boundary conditions listed below (Stoker 1947):

$$\frac{\partial^2 \varphi}{\partial x^2} + \frac{\partial^2 \varphi}{\partial y^2} = 0, \tag{2.1}$$

$$\frac{\partial \varphi}{\partial y} - \varphi = 0 \quad \text{in } y = 0, \tag{2.2}$$

$$\frac{\partial \varphi}{\partial \boldsymbol{n}} = 0 \quad \text{in } y = -h(x) = -x\beta, \tag{2.3}$$

where $\boldsymbol{n}$ denotes the unit vector normal to the bottom and h is the water depth. The function φ has been computed by using the solution of Stoker (1947), which can be applied when the angle of the slope γ ($\beta = \tan(\gamma)$) can be expressed as $\gamma = \pi/(2n)$, where n is a natural number. The solution uses the theory of the analytic functions $f(z) = \varphi + \mathrm{i}\psi$ of the complex variable $z = x + \mathrm{i}y$, where, in the present case, the real part of $f(z)$ is the potential function and the imaginary part is the streamfunction. An analytic function already satisfies the Laplace equation, therefore a solution is found if an analytic function which also satisfies the boundary conditions is determined. Hence, the boundary conditions are used to derive a differential equation for $f(z)$. Preliminarily, (2.2) and (2.3) are reformulated in terms of $f(z)$ respectively as follows:

$$\left(\frac{\partial}{\partial y} - 1\right)\varphi = \mathrm{Re}\left(\frac{\partial}{\partial y} - 1\right) f(z) = \mathrm{Re}\left(\mathrm{i}\frac{\mathrm{d}}{\mathrm{d}z} - 1\right) f(z) = \mathrm{Re}\, L_{2n} f(z) = 0, \tag{2.4}$$

$$\frac{\partial \varphi}{\partial \boldsymbol{n}} = \mathrm{Re}\left(\frac{\partial f}{\partial \boldsymbol{n}}\right) = \mathrm{Re}\left(-\mathrm{i}\mathrm{e}^{-\mathrm{i}\pi/2n}\frac{\mathrm{d}}{\mathrm{d}z}\right) f(z) = \mathrm{Re}\, L_1 f(z) = 0, \tag{2.5}$$

where the bottom is described by $z = r\mathrm{e}^{-\mathrm{i}\pi/2n}$ ($r = |z|$) and L_{2n} and L_1 are two differential operators. Additional $2n - 2$ operators $(L_2, L_3, \ldots, L_{2n-1})$ are defined such that the operator $L = L_1 \cdot L_2 \cdot L_3 \cdot \cdots \cdot L_{2n}$ applied to $f(z)$ produces a function $F(z)$ whose real part vanishes both at the free surface and at the bottom. A key feature of L is its invariance under an exchange of position of the operators L_j. By considering the properties of $F(z)$ along with the fact that the fluid domain is a sector of

https://doi.org/10.1017/jfm.2012.181 Published online by Cambridge University Press

angle $\pi/2n$, the function $F(z)$ can be extended analytically over the boundaries of the domain through successive reflections, thus obtaining a function regular in the entire plane except in the origin, where a pole at most of order $2n$ is present. The detailed analysis provided by Stoker (1947) shows that $F(z) = A_{2n}\mathrm{i}/z^{2n}$, where A_{2n} is an arbitrary real constant. The solution of the homogeneous part of the differential equation $Lf(z) = F(z)$ is a function $f_1(z)$ which is everywhere regular, while the solution $f_2(z)$ of the non-homogeneous equation contains a logarithmic singularity in the origin, denoting the presence of a source or a sink. After introducing the coefficients $\beta_k = \mathrm{e}^{\mathrm{i}\pi(k/n+1/2)}$, the functions f_1 and f_2 are given by

$$f_1(z) = \sum_{k=1}^{n} c_k \mathrm{e}^{z\beta_k}, \quad f_2(z) = \sum_{k=1}^{n} \frac{c_k}{\pi}\left(\mathrm{e}^{z\beta_k}\int_{\infty}^{z\beta_k}\frac{\mathrm{e}^{-\xi}}{\xi}\,\mathrm{d}\xi - \pi\mathrm{i}\mathrm{e}^{z\beta_k}\right), \tag{2.6}$$

where the path of integration in the second part of (2.6) is shown in figure 2 of Stoker (1947). In order that f_1 and f_2 satisfy (2.4) and (2.5), c_k must be computed as follows:

$$c_k = \mathrm{e}^{\mathrm{i}\pi[(n+1)/4-k/2]}\cot\left(\frac{\pi}{2n}\right)\cot\left(\frac{2\pi}{2n}\right)\cdots\cot\left(\frac{(k-1)\pi}{2n}\right), \quad k = 2, 3, \ldots, n. \tag{2.7}$$

For c_1 we have $c_1 = c_n^+$, where $+$ means complex conjugate. Upon reintroduction of the time factor, the potentials φ_1 and φ_2, given by the real parts of (2.6), provide the potentials of two standing waves. It can be shown that at $x = \infty$ the two solutions are out of phase, being their asymptotic behaviour: $\varphi_1 \sim \cos(x + (n-1)\pi/4)$ and $\varphi_2 \sim \sin(x+(n-1)\pi/4)$. The logarithmic singularity of $f_2(z)$ is essential in determining the previous feature, thanks to which wave solutions that at $x = \infty$ behave as deep water waves propagating onshore (Φ_i) or offshore (Φ_r), can be obtained,

$$\Phi_i = \varphi_1\mathrm{e}^{\mathrm{i}(t+\alpha)} - \varphi_2\mathrm{e}^{\mathrm{i}(t+\alpha-\pi/2)}; \quad \Phi_r = K(\varphi_1\mathrm{e}^{\mathrm{i}(t+\alpha_r)} + \varphi_2\mathrm{e}^{\mathrm{i}(t+\alpha_r-\pi/2)}), \tag{2.8}$$

where K is the reflection coefficient, α and α_r are the phases of the incident and of the reflected waves, respectively. In the first of (2.8) the constant factor is fixed to 1 in order to meet the dimensionless amplitude of the incoming wave at $x = \infty$. When both progressive and reflected waves are present, the potential Φ is obtained by adding Φ_r to Φ_i. In particular, the potential of a standing wave is obtained by setting the value of K to 1. We can imagine that a standing wave is physically generated by a progressive wave which is fully reflected from a wall placed in one of the antinodes. For convenience, the irrotational velocity $(U, V) = \nabla\Phi$ will be expressed as $(U, V) = (\hat{U}, \hat{V})\mathrm{e}^{\mathrm{i}t}$.

After introducing the bottom boundary layer, we observe that at the order a_0 a steady streaming is generated which, at the outer edge of this layer, is given by the first of (2.9) (Mei, Stiassnie & Yue 2005*b*), where r and $\hat{U}_r$ are the coordinate and the irrotational velocity along the bottom, respectively. Analogously, at the same order of approximation, in the free surface boundary layer a mean vorticity is generated which, at the outer edge of this layer, is given by the second part of (2.9) (Longuet-Higgins 1953; Liu 1977):

$$\overline{u}_r = -\left(\widehat{U}_r\frac{\partial\widehat{U}_r^+}{\partial r}\right)_{y=-h}\left[\frac{3}{4}(\mathrm{i}+1)\right]; \quad \overline{\omega} = 2\mathrm{i}\left(\frac{\partial\hat{U}^+}{\partial x}\frac{\partial\hat{V}}{\partial x}\right)_{y=0}. \tag{2.9}$$

In order to compute the mass transport in the core region, the equation of the second-order mean vorticity must be solved (Longuet-Higgins 1953; Dore 1976) along with

https://doi.org/10.1017/jfm.2012.181 Published online by Cambridge University Press

boundary conditions defined by (2.9). Since the shape of the domain is that of a circular sector, we write such equation in the polar coordinate system (r, θ) as

$$\left(u_{sr} + \frac{1}{r}\frac{\partial \bar{\psi}}{\partial \theta}\right)\frac{\partial \bar{\omega}}{\partial r} + \left(u_{s\theta} - \frac{\partial \bar{\psi}}{\partial r}\right)\frac{1}{r}\frac{\partial \bar{\omega}}{\partial \theta} = D\left[\frac{1}{r}\frac{\partial}{\partial r}\left(r\frac{\partial \bar{\omega}}{\partial r}\right) + \frac{1}{r^2}\frac{\partial^2 \bar{\omega}}{\partial \theta^2}\right], \quad (2.10)$$

where $D = (\delta/a_0)^2/2$, u_{sr} and $u_{s\theta}$ are the components of the Stokes drift velocity (Dore 1976) along the r and the θ directions respectively and $\bar{\psi}$ is the streamfunction of the mean Eulerian velocity. The system of differential equations that describes the mean vorticity is completed by the equation that links the vorticity to the stream function,

$$\bar{\omega} = -\left[\frac{1}{r}\frac{\partial}{\partial r}\left(r\frac{\partial \bar{\psi}}{\partial r}\right) + \frac{1}{r^2}\frac{\partial^2 \bar{\psi}}{\partial \theta^2}\right]. \quad (2.11)$$

In the present study the parameter D takes values much smaller than 1, therefore nonlinear terms in (2.10) are important and a numerical approach must be used to solve the system (2.10)–(2.11).

In principle the integration of (2.10)–(2.11) should be performed in a domain that extends from $x = x_1$, near the shoreline, up to ∞ offshore. However, since the solution is sought numerically, the domain must be truncated at a certain position $x = x_2 > x_1$. Along the boundary of this domain appropriate conditions for $\bar{\psi}$ and $\bar{\omega}$ must be introduced.

The bottom is a streamline both under a Lagrangian and an Eulerian point of view, therefore here we set $\psi_L = \bar{\psi} = 0$, where ψ_L is the streamfunction of the Lagrangian mass transport. We recall that at the order a_0 the relation $\psi_L = \bar{\psi} + \psi_s$ holds, where ψ_s is the streamfunction of the Stokes drift (Longuet-Higgins 1953; Dore 1976).

The mean free surface is a streamline in a Lagrangian frame of reference but not in an Eulerian one. A reasoning based on mass conservation, similar to that outlined in Blondeaux *et al.* (2002), shows that the streamfunction at the free surface is given by

$$(\bar{\psi})_{y=0} = \frac{\mathrm{i}}{2}(\hat{U}\hat{V}^{+})_{y=0}. \quad (2.12)$$

At the free surface the vorticity is given by the second of (2.9), while at the bottom the vorticity is not known *a priori* as it depends on the flow in the interior. Therefore, we write (2.11) at $y = -h$ in order to link the vorticity on the boundary to the flow in the interior as follows:

$$(\bar{\omega})_{y=-h} = -\left(\frac{1}{r^2}\frac{\partial^2 \bar{\psi}}{\partial \theta^2}\right)_{y=-h}. \quad (2.13)$$

Finally, the boundary conditions on the side boundaries are introduced. On the wall placed near the beach ($x = x_1$), where the wave undergoes a full reflection, the boundary condition for the streamfunction is $\bar{\psi} = 0$. The offshore boundary at $x = x_2$ is an artificial boundary, therefore no natural boundary conditions can be identified here. Under such circumstances a boundary condition must be introduced with the requirement that it must not affect the solution far from the boundary. Therefore, at $x = x_2$ we introduced the condition $\partial^2 \bar{\psi}/\partial r^2 = 0$, which was found to fulfil the mentioned requirement.

Summarizing, the physical features which affect the mass transport in the core region are the steady streaming at the outer edge of the bottom boundary layer (first (2.9)), the mean vorticity at the outer edge of the free surface boundary layer (second (2.9)), the Stokes drift velocity in (2.10) and the flow rate of the Eulerian mass

https://doi.org/10.1017/jfm.2012.181 Published online by Cambridge University Press

transport given by (2.12). All of the previous quantities depend on the first-order irrotational flow and, except the steady streaming at the outer edge of the bottom boundary layer, vanish in the case of a standing wave.

The equations have been discretized by finite difference approximations. The numerical mesh is made up of n_r and n_θ grid points along the r and the θ directions respectively. The spatial derivatives have been approximated by centred finite differences. Unless otherwise stated, the convective term has been computed by the second-order numerical scheme of Arakawa (1966), which conserves both energy and enstrophy.

The solution has been computed iteratively, by introducing in the left-hand side of (2.10) a fictitious time derivative and advancing the solution in time until a steady condition has been attained. The time advancement has been carried out explicitly, except the second derivative in the θ direction which was treated implicitly in order to contain the viscous numerical instabilities. After taking into account the steady streaming at the bottom, given by the first part of (2.9), the vorticity boundary condition (2.13) has been converted into finite difference form according to the method proposed by Thom (1928).

3. Discussion of the results

A first validation of the numerical model has been carried out for a progressive wave ($K = 0$) on constant depth, characterized by a vanishing convective term. The Lagrangian mean velocity computed by the model was found to be in a very good agreement with the diffusion solution of Longuet-Higgins (1953). A more significant validation would require us to consider a reference case characterized by a non-vanishing convective term. Specifically, for the aim of the present study, it would be appropriate to consider a wave propagating over a sloping beach and fully reflected from a wall. However, to the best of the authors' knowledge, no experimental data are available in the literature for a standing wave field over a sloping bottom. Therefore, the validation has been carried out by reproducing the experimental results of Hwung & Lin (1990), who performed measurements of the mass transport under progressive waves propagating along an artificial beach of slope 1:15, outside the surf zone, without the presence of any wall. In order to simulate this case, at $x_1 = 2$ the boundary condition which forces the vanishing of the second derivatives of $\bar{\psi}$ with respect to r has been introduced as well as at the offshore boundary which has been placed at $x_2 = 22$. Owing to the condition $\partial^2\overline{\psi}/\partial r^2 = 0$ introduced at the onshore boundary, where inflow and outflow coexist, the need to increase the numerical stability of the iterative procedure used to solve the system (2.10)–(2.11) has emerged. Therefore, only for this case, the convective term has been computed by upwind finite differences (Roache 1972), which exhibit the desired stability properties. The numerical mesh has been generated by fixing $n_r = 400$ and $n_\theta = 100$.

As shown in figure 1, the model is in a fairly good agreement with the experiments. A larger discrepancy is observed near the beach, probably because of the turbulence generated by the wave breaking, not reproduced by the present model, and advected offshore by the mass transport. In figure 1 we further observe that far from the bottom the velocity profiles are substantially constant as convective effects prevail in this region. On the other hand, near the bottom a balance between viscous and convective effects takes place, therefore a second boundary layer develops whose thickness is of order δ/a_0.

https://doi.org/10.1017/jfm.2012.181 Published online by Cambridge University Press

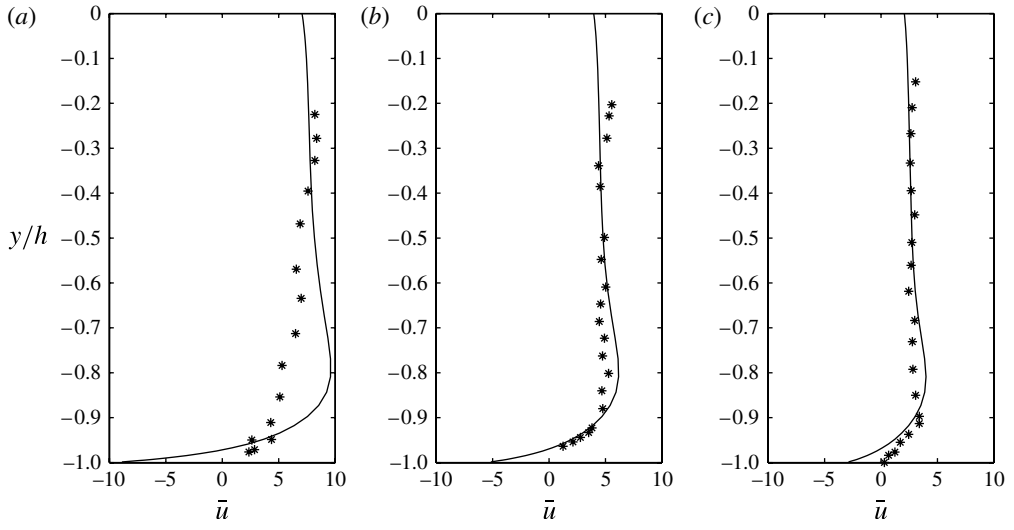


FIGURE 1. Comparison between the horizontal velocity profiles computed by the present model and those measured by Hwung & Lin (1990) for $T^* = 1.41$ s, $a_0^* = 5.3$ cm, $D = 2.7 \times 10^{-4}$, beach slope 1:15, with: (*a*) $h^* = 9.8$ cm, (*b*) $h^* = 13$ cm and (*c*) $h^* = 17.4$ cm. Continuous line: numerical results; stars: experimental measurements.

We begin the study of the mass transport under standing waves by considering an incoming wave characterized by $D = 0.01$ and a beach with slope of 1:10. The wave is fully reflected from a wall, placed at $x_1 = 2.46$, on which a steady streaming is generated because of the no slip condition. The computation of such steady streaming is performed by the first of (2.9), where $\hat{U}_r$ is replaced with the irrotational velocity at the wall and r with the coordinate along the wall. This steady streaming is directed towards the bottom, it takes the largest value at the free surface and vanishes at the bottom. In the present computations the offshore boundary has been placed at $x_2 = 22.9$ and a grid with $n_r = 600$ and $n_\theta = 100$ has been introduced.

In figure 2(*a*) we observe that the flow is organized in recirculating cells. At the outer edge of the bottom boundary layer the mean velocity is directed from the nodes towards the antinodes. However, as also reported by Mei *et al.* (2005*b*), at the bottom the direction reverses. Therefore, in the case of a sandy bottom, sediments are eroded from the antinodes and piled up at the nodes where the crest of a bar is formed. Since the wall is placed in an antinode, this phenomenon can strongly affect the wall stability.

The mean velocity is upward directed under the antinodes and downward directed under the nodes. Upward convection of vorticity is then generated under the antinodes, i.e. along the boundary between a positive cell and the negative one placed just offshore from the former. The large values of vorticity under the antinodes explain why the maximum of $|\overline{\psi}|$ of a positive cell and that of the negative cell placed just offshore from the former, are close to each other. Indeed, according to (2.11), large values of the vorticity should cause a clustering of the streamlines.

We also note a very small positive cell adjacent to the wall. This cell, in the following referred as the wall cell, is due to the steady streaming developing on the wall.

https://doi.org/10.1017/jfm.2012.181 Published online by Cambridge University Press

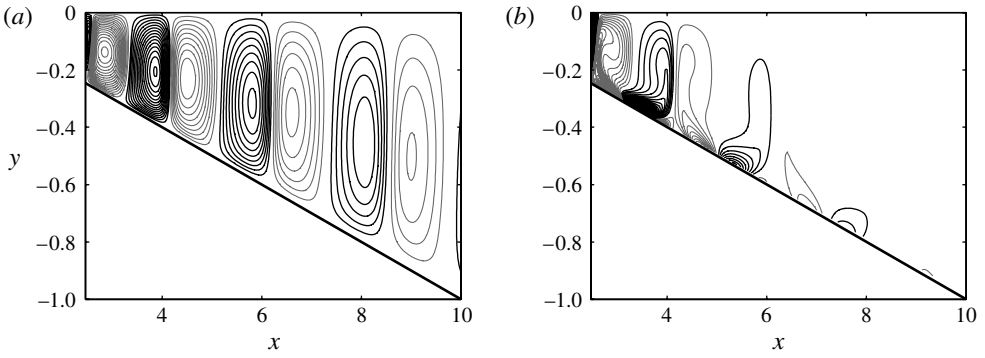


FIGURE 2. Streamlines (*a*) and vorticity (*b*) of the mean Eulerian flow under a progressive wave fully reflected at $x_1 = 2.46$, over a slope of 1:10, for $D = 0.01$: (*a*) $\Delta\overline{\psi} = 0.025$ and (*b*) $\Delta\overline{\omega} = 6$. Black line: positive values; grey line: negative values.

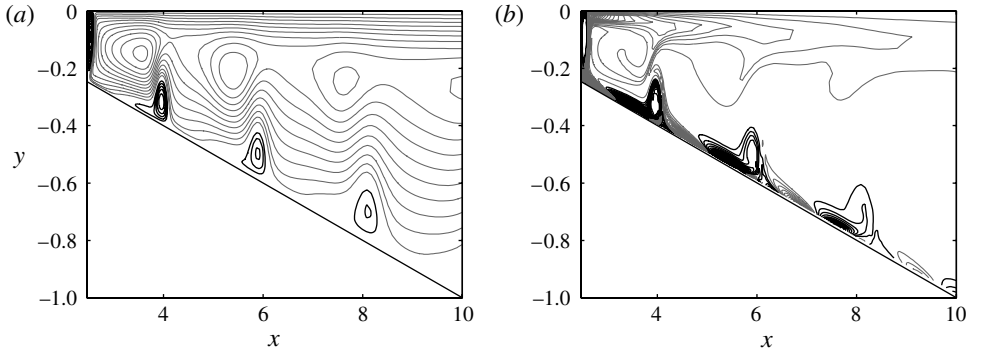


FIGURE 3. Streamlines (*a*) and vorticity (*b*) of the mean Eulerian flow under a progressive wave fully reflected at $x_1 = 2.46$, over a slope of 1:10, for $D = 0.001$: (*a*) $\Delta\overline{\psi} = 0.025$ and (*b*) $\Delta\overline{\omega} = 6$. Black line: positive values; grey line: negative values.

In order to examine the effect of a decrease of the parameter D, a case characterized by the same geometrical parameters as the previous case but in the value of D an order of magnitude smaller has been considered. The number of gridpoints (n_r, n_θ) has been set to (800, 100). The flow is shown in figure 3, where the most remarkable result is the coalescence of the negative cells into a single large cell and the weakening of the positive cells. Since in the case of standing waves the Stokes drift vanishes, the contour lines in figure 3(*a*) are also streamlines of the Lagrangian mass transport. Therefore, a cross-shore drift is generated where fluid particles and suspended materials move offshore near the free surface and onshore near the bottom. Regions of clockwise recirculation are however still present in the middle of the water depth. In figure 3(*b*) offshore advection of negative vorticity is present in the upper part of the fluid domain. Such vorticity is mainly produced at the bottom, near the wall.

The independence of the coalescence phenomenon on the position x_2 of the offshore boundary has been demonstrated by computations carried out for different values of x_2. In all of the examined cases the negative cells coalesced as shown in figure 3.

https://doi.org/10.1017/jfm.2012.181 Published online by Cambridge University Press

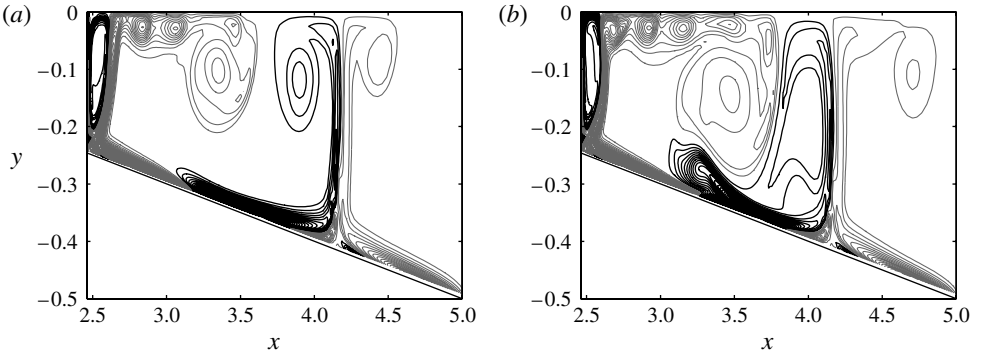


FIGURE 4. Vorticity of the mean Eulerian flow under a progressive wave fully reflected at $x_1 = 2.46$, at two times during the false transient, over a slope of 1:10, for $D = 0.001$; (*a*) $t = 1$, (*b*) $t = 1.5$. $\Delta\overline{\omega} = 12$. Black line: positive values; grey line: negative values.

The coalescence has also been confirmed by a computation performed by fixing the offshore boundary between two cells and imposing the boundary condition $\bar{\psi} = 0$.

Insights about the physical mechanism behind the coalescence phenomenon can be gained by analysing the vorticity distribution at two times during the false transient, when a steady condition has not yet been attained (figure 4). In figure 4(*a*) the vorticity in the first negative cell is stronger than that in the first positive cell as in the former the water is shallower and the vorticity generated at the bottom larger. The strong negative vorticity induces a downward motion of the fluid in the positive cell, which is incorporated by the negative cell, as can be noted in figure 4(*b*). When the positive cell becomes small enough, the negative cell merges with the negative one placed just offshore and feeds it with negative vorticity. Then the phenomenon propagates offshore causing the merging of all of the negative cells.

Present results suggest that the coalescence is due to the seaward decrease of the vorticity induced by the sloping bottom, hence it should disappear when the bottom is horizontal. The phenomenon could also be influenced by the wall cell. In order to check the importance of these effects, the mean flow induced by a sea wave propagating over a constant depth and fully reflected from a wall has been computed for $D = 0.001$ and $h = 0.25$. The wall has been placed at $x_1 = 0$ and the offshore boundary at $x_2 = 6.77$. The values of n_r and n_θ have been set equal to 800 and 200, respectively. Figure 5 shows that no coalescence has taken place, thus confirming that the merging is due to the seaward decrease of the vorticity when the slope is not equal to zero. In figure 5 we can also observe that the wall cell mainly affects the size of the first two cells.

At this stage the question arises whether non-zero values of the slope exist for $D = 0.001$ such that the negative cells do not coalesce. This question has been tackled by analysing the results of two computations carried out by fixing the value of the slopes to 1:26 and 1:35 respectively. When reducing the slope, the wall has been moved offshore in order to maintain a water depth of $\sim$0.25 at the position of the wall.

In figure 6(*a*), for a slope of 1:26, the first two negative cells have coalesced while all of the others remained separated. Figure 6(*a*) clearly highlights that each negative cell tends to compress the adjacent positive cell. Finally, for a slope of 1:35

https://doi.org/10.1017/jfm.2012.181 Published online by Cambridge University Press

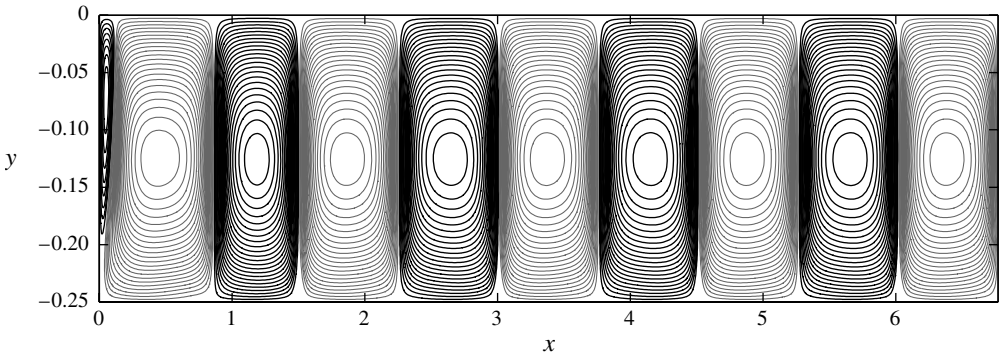


FIGURE 5. Streamlines of the mean Eulerian flow induced by a progressive wave propagating over a horizontal bottom and fully reflected at $x = 0$, for $D = 0.001$: $\Delta\overline{\psi} = 0.025$. Black line: positive values; grey line: negative values.

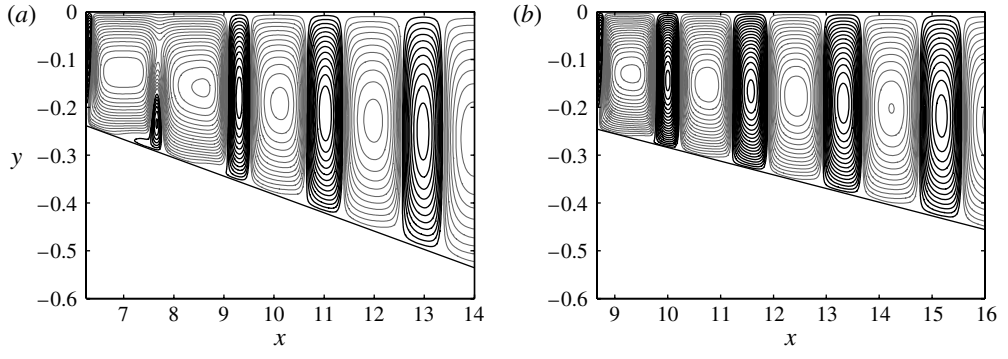


FIGURE 6. Streamlines of the mean Eulerian flow induced by progressive waves propagating over a sloping bottom for $D = 0.001$; (*a*) $x_1 = 6.25$, slope = 1:26; (*b*) $x_1 = 8.66$, slope = 1:35. $\Delta\overline{\psi} = 0.25$. Black line: positive values; grey line: negative values.

in figure 6(*b*), no merging is observed. Therefore, for $D = 0.001$ a small value of the slope exists such that merging does not take place.

The relative importance of the wall cell increases when the wall is moved offshore and the bottom slope is kept constant. Indeed, when the depth increases the steady streaming on the wall acts over a larger extension, therefore the recirculating cell becomes stronger, while the cells induced by the steady streaming at the bottom are weakened. We can observe the structure of the flow when the wall is moved offshore in figure 7, where results for a wall placed at $x = 16.80$ are shown. In figure 7(*a*) a large wall cell can be observed which occupies the place of the first negative cell but it is not likely to undermine the mechanism of merging. It is interesting that in figure 7(*b*) the positive vorticity in the wall cell is produced in the upper part of the wall only, i.e. in the range $-0.25 < y < 0$. The positive vorticity enhances the production of negative vorticity at the bottom which is convected upwards and then offshore.

Information about the influence of the parameter D and of the slope β on the merging phenomenon are shown in figure 8 for a water depth at the position of the

https://doi.org/10.1017/jfm.2012.181 Published online by Cambridge University Press

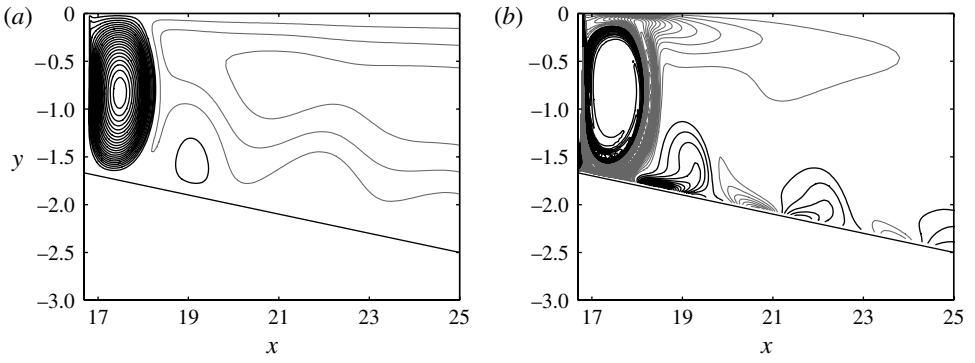


FIGURE 7. Streamlines (*a*) and vorticity (*b*) of the mean Eulerian flow induced by a progressive wave fully reflected at $x_1 = 16.8$, over a slope of 1:10, for $D = 0.001$: (*a*) $\Delta\overline{\psi} = 0.01$; (*b*) $\Delta\overline{\omega} = 0.1$. Black line: positive values; grey line: negative values.

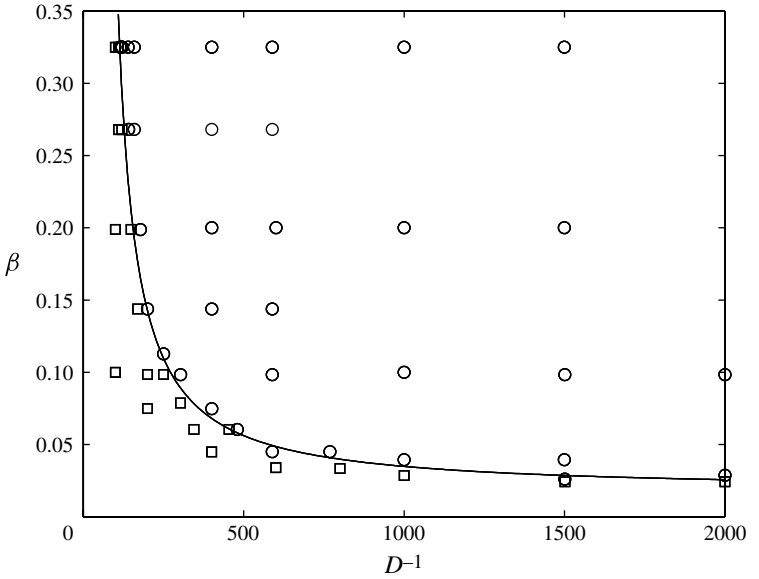


FIGURE 8. No merging □ and merging ◯ of the recirculating cells of the mass transport under standing waves over a sloping beach, for a depth at the position of the wall equal to 0.25. The continuous line approximates the boundary between the region of cell merging and the region where the classical recirculating cell structure is observed.

wall equal to 0.25. When D^{-1} is small, very large values of β are necessary in order to produce the merging phenomenon. We estimated that for values of D^{-1} smaller than $\sim$110, merging does not take place, no matter how large β is. This finding shows that, even though the rate of the seaward decrease of vorticity grows when the slope increases, for low values of D^{-1} viscous forces are so strong as to inhibit cell merging. The curve in figure 8 approximates the boundary between the region of cell merging and the region where the classical recirculating cell structure is observed. The equation of this curve is $\beta = 32/\left(D^{-1} - 45\right)^{1.1} + 0.018$ and is valid when $D^{-1} > 110$.

https://doi.org/10.1017/jfm.2012.181 Published online by Cambridge University Press

When D^{-1} increases merging takes place for smaller and smaller values of β. However, present analysis is no longer reliable for very large values of D^{-1} as the flow is expected to become turbulent. How the depth at the position of the wall affects the picture shown in figure 8 has not been investigated in detail. However, on the basis of few results, we expect that higher values of the depth cause a displacement of the curve towards higher values of β.

4. Conclusions

The mass transport induced by progressive waves propagating over a sloping beach and fully reflected from a wall has been studied. For sufficiently large values of the parameter D, representing the order of magnitude of the ratio between viscous and convective effects, the flow is organized into the well-known recirculating cell structure.

By fixing the beach slope and reducing the value of D, negative and positive cells interact with each other. As a result of this interaction, negative cells incorporate the fluid of the positive cells.

Under such circumstances the flow is characterized by positive cells confined near the bottom and negative cells merged into one large cell. Inside this cell, near the bottom the fluid particles move onshore while near the free surface they move offshore. The seaward decrease of the vorticity generated at the bottom, along with high values of inertia forces compared with viscous forces, appear to be the reason of the merging phenomenon.

By keeping the value of D fixed and reducing the slope, the merging of only a few cells near the wall is observed for small slopes, while, for very small slopes, no merging is observed although the negative cells are larger because they tend to incorporate the fluid of the positive cells. As expected, in the case of a horizontal bottom, positive and negative cells have the same size, except the first two cells near the wall because they are affected by the wall cell, generated by the steady streaming on the wall.

When the depth at the wall location increases, the wall cell becomes much stronger then the other cells, however, it does not compromise the mechanism that gives rise to the coalescence of the negative cells.

Finally, the flow characteristics in the Reynolds number–beach slope plane have been analysed for a depth at the position of the wall equal to 0.25. It has been shown that the cells merge for a sufficiently high values of the slope, if the Reynolds number (D^{-1}) is larger than $\sim$110. When the Reynolds number is smaller than the previous value, merging does not take place, no matter how large is the slope. The explanation for this finding is that even though the rate of seaward decrease of vorticity grows when the slope increases, for low values of the Reynolds number the viscous forces are so strong as to prevent cell merging.

REFERENCES

ARAKAWA, A. 1966 Computational design for long-term numerical integration of the equations of fluid motion: two-dimensional incompressible flow. Part 1. *J. Comput. Phys.* **1** (1), 119–143.

BLONDEAUX, P., BROCCHINI, M. & VITTORI, G. 2002 Sea waves and mass transport on a sloping beach. *Proc. R. Soc. Lond.* A **458**, 2053–2082.

CARTER, T. G., LIU, P. F.-L. & MEI, C. C. 1973 Mass transport by waves and offshore sand bedforms. *J. Waterways Harbors Div. ASCE* **99**, 165–184.

CRAIK, A. D. D. 1982 The drift velocity of water waves. *J. Fluid Mech.* **116**, 187–205.

https://doi.org/10.1017/jfm.2012.181 Published online by Cambridge University Press

DORE, B. D. 1976 Double boundary layers in standing surface waves. *Pure Appl. Geophys.* **114**, 629–637.

HADDON, E. W. & RILEY, N. 1983 A note on the mean circulation in standing waves. *Wave Motion* **5**, 43–48.

HUNT, J. N. & JOHNS, B. 1963 Currents induced by tides and gravity waves. *Tellus* **15**, 343–351.

HWUNG, H. H. & LIN, C. 1990 The mass transport of waves propagating on a sloping bottom. In *Proceedings of XXII International Conference Coastal Engineering*, pp. 544–556. ASCE.

ISKANDARANI, M. & LIU, P. L.-F. 1991*a* Mass transport in two-dimensional water waves. *J. Fluid Mech.* **231**, 395–415.

ISKANDARANI, M. & LIU, P. L.-F. 1991*b* Mass transport in three-dimensional water waves. *J. Fluid Mech.* **231**, 417–437.

LAU, J. & TRAVIS, B. 1973 Slow varying stokes waves and submarine longhshore bar. *J. Geophys. Res. Oceans* **78**, 4489–4497.

LIU, P. L.-F. 1977 Mass transport in the free surface boundary layers. *Coastal Engng* **1**, 207–219.

LONGUET-HIGGINS, M. S. 1953 Mass transport in water waves. *Phil. Trans. R. Soc. Lond.* A **345**, 535–581.

MEI, C. C., STIASSNIE, M. & YUE, D. K.-P. 2005*a Theory and Applications of Ocean Surface Waves Part 1: Linear Aspects*. World Scientific.

MEI, C. C., STIASSNIE, M. & YUE, D. K.-P. 2005*b Theory and Applications of Ocean Surface Waves Part 2: Nonlinear Aspects*. World Scientific.

RILEY, N. 2001 Steady streaming. *Annu. Rev. Fluid Mech.* **33**, 43–65.

ROACHE, P. J. 1972 *Computational Fluid Dynamics*. Hermosa Publishers.

STOKER, J. J. 1947 Surface waves in water of variable depth. *Q. Appl. Maths* **5**, 1–54.

THOM, A. 1928 An investigation of fluid flow in two dimensions. *Tech. Rep.* 1194. Aerospace Research Center UK.

WEN, J. & LIU, P. L.-F. 1994 Mass transport under partially reflected waves in a rectangular channel. *J. Fluid Mech.* **226**, 121–145.

https://doi.org/10.1017/jfm.2012.181 Published online by Cambridge University Press